IEEE Access
Multidisciplinary | Rapid Review | Open Access Journal

Received October 17, 2018, accepted November 20, 2018, date of publication November 23, 2018,
date of current version December 27, 2018.

Digital Object Identifier 10.1109/ACCESS.2018.2883081

Three-Dimensional Path Following of an Underactuated AUV Based on Neuro-Adaptive Command Filtered Backstepping Control

JINQIANG WANG, CONG WANG, YINGJIE WEI, AND CHENGJU ZHANG
School of Astronautics, Harbin Institute of Technology, Harbin 150001, China

Corresponding author: Cong Wang (alanwang@hit.edu.cn)

This work was supported by the National Natural Science Foundation of China (NSFC) Under Grant 11672094.

ABSTRACT This paper investigates the problem of path following control of the underactuated autonomous underwater vehicles in the presence of model uncertainties and external disturbances. With the three-dimensional path following error model established based on virtual guidance method, a path following robust control system is proposed using the command filtered backstepping control, neural networks, and adaptive control techniques. Then, a Lyapunov-based stability analysis demonstrates that all the signals are bounded and path following errors ultimately converge to a neighborhood of the origin. Following advantages are highlighted in this paper: 1) the derivative of virtual control is obtained via a second-order filter, which avoids explosion of complexity in the traditional backstepping design, and filters out high frequency measurement noise to keep the control system more robust, and a filtered error compensation loop is developed to guarantee the approximation precision between the virtual control signals and the filtered signals and 2) the presented controller is easily put into practice without any former knowledge of vehicle parameters and external environmental disturbances. Finally, the simulations are conducted, and results illustrate the effectiveness and good robustness of the proposed control system through a new class of flying wing autonomous underwater vehicle.

INDEX TERMS Underactuated AUV, path following, model uncertainty, command filtered backstepping, neural networks.

I. INTRODUCTION

The control problems of the underactuated autonomous underwater vehicles (AUVs) has attracted significant attention from the research community due to their wide applications in the exploration of ocean resource and military affairs, such as oceanography, surveillance, ocean floor survey, seafloor mapping, deep sea archaeology, oil and gas industry [1]–[5]. A typical and indispensable task is to follow a prescribed path without time constraints and complete some missions [6], [7]. Due to the consideration of weight, cost and energy consumption, most autonomous underwater vehicles are underactuated, which signifies that they lack independent control inputs in the whole degrees of freedom, and the absence of actuator in sway and heave actuation presents great challenges on the controller design. In addition, the AUVs usually work in the harsh ocean environment and their motions are strongly influenced by perturbations including hydrodynamic parameters and external disturbances such as waves, ocean currents and so on [8], [9]. Therefore, the path following control problem for the underactuated AUVs is of great challenge.

Much of the early work for the path following problem of the underactuated AUVs were publisheded in a huge number of academic papers. Approaches based on the line-of-sight (LOS) guidance were very successfully applied in the horizontal path following [10]–[14]. Moreover, backste- pping control approach was also employed widely in the path following control problem of the underactuated AUVs [15]–[17]. A novel method based on Lyapunov stability theory and feedback gain backstepping technology for the marine surface vehicles has been presented in [18]. A state feedback backstepping control algorithm has been proposed for the path following problem of underactuated AUVs [19]. The robust adaptive fuzzy sliding control scheme with fully unknown parameters has been presented in [20] and [21]. A novel direct controller based on adaptive fuzzy technology with unknown parametric dynamics was designed in [22] and [23], and an adaptive robust online constructive

fuzzy control method was employed to deal with the model uncertainties and unknown external disturbances. In [24], the adaptive neural network (NN) controller based on the Lyapunov stability theory has been developed to realize the path following of the underactuated AUVs in the presence of parameter uncertainties and unknown external disturbances. In [25], a robust controller for the horizontal path following problems of underactuated AUVs was designed based on the dynamic surface control (DSC) technology, and the neural network system was employed to process the vehicle uncertainties. Unfortunately, it is very necessary to indicate that most of previously published researches concentrate on the path following problems only in the horizontal plane. However, in the three-dimensional space, the path following problem is more difficult due to the fact that the dynamics of AUVs is more complicated and the number of degrees of freedom increases, which makes the control scheme design more challenging [26]. Therefore, only a few researchers have investigated this control problem. In [27], a new kinematic controller based on backstepping and Lyapunov techniques was proposed to deal with the vehicle dynamics. In [28], the cascade system theory and backstepping method were employed to develop controllers based on the LOS, which can reduce the complexities of the controllers, but not suit for the general desired path. In [29], an adaptive nonlinear controller was presented based on the backstepping and sliding mode control, and the fuzzy logic theory was used to deal with the problems of vehicle uncertainties and external environment disturbances in the control system. In [30], a nonlinear controller based on the command filtered backstepping was presented, which can greatly reduce the computational complexities of the traditional backstepping approach, but not consider the parameter uncertainties and environmental disturbances thus restricting its applications in practice. To sum up, all of the aforementioned controllers at least suffer from one of the following shortcomings:

(i) Most of previously designed control scheme for the path following control of the underactuated AUVs only concentrate on their planar motions which are not suitable for the three-dimensional problem.
(ii) The second problem is about the intrinsic explosion of complexities in the traditional back-stepping method.
(iii) The previous controllers generally assume that both the parameter uncertainties and external disturbances are not considered or are linear-in-parameter (LIP), which restricts the application of AUVs in practice.

Toward this end, this paper has proposed a nonlinear path following control scheme based on the command filtered backstepping approach for three-dimensional path following problems of the underactuated AUVs, and the neuro-adaptive control techniques are employed to deal with the problems of parameter uncertainties in the control system.

The remainder of this paper is arranged as follows. The preliminary and problem statement are presented in Section II. The robust controller design for the three-dimensional path following of an underactuated AUV is proposed in Section III. The stability analysis for the overall control system is presented in Section IV. Simulation results to evaluate the proposed controller performance are presented in Section V. Finally, the conclusions and futurework are drawn in Section VI.

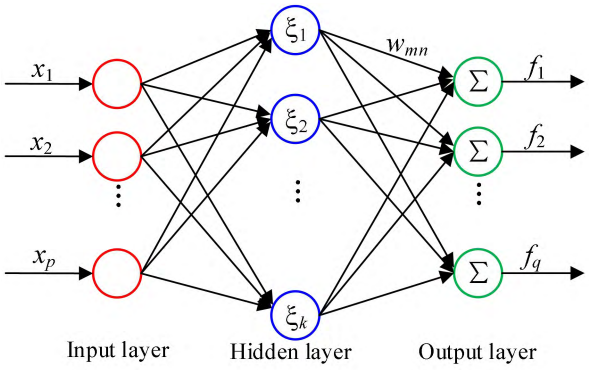

FIGURE 1. The structure of RBF neural network.

II. PRELIMINARY AND PROBLEM STATEMENT

A. NEURAL NETWORKS

Neural networks are widely applied in the design of various robotic controllers due to their intrinsic capabilities in function approximations. Among them, the radial basis function neural networks (RBFNNs) are very popular due to their simplicity and linear parameterization [31]. The structure of a three-layer RBFNN is illustrated in Figure 1.

For a arbitrary continuous function $f(x) : \Re^p \to \Re^q$, there is a RBFNN such that

$$\begin{cases} f_m(x) = \sum_{n=1}^{k} w_{mn}\xi_n(x) + \varepsilon_{wm}(x), \\ \qquad\qquad m = 1, 2, 3, \ldots, q, \ \forall x \in \Re^p \\ \xi_n(x) = \exp(-(x - \boldsymbol{\mu}_n)^2/\lambda_n^2), \quad n = 1, 2, 3, \ldots, k \end{cases} \tag{1}$$

which can be also expressed as $\boldsymbol{f}(\boldsymbol{x}) = \boldsymbol{W}\xi(\boldsymbol{x}) + \boldsymbol{\varepsilon}_w(\boldsymbol{x})$ where $\boldsymbol{x} = [x_1, x_2, \ldots, x_p]^{\mathrm{T}}$ is the input vector, $\boldsymbol{f}(\boldsymbol{x}) = [f_1(\boldsymbol{x}), \ldots, f_p(\boldsymbol{x})]^{\mathrm{T}}$ represents the output vector. $\boldsymbol{W} \in \Re^{q\times k}$ is the NN weights matrix, and $\boldsymbol{\xi}(\boldsymbol{x}) = [\xi_1(\boldsymbol{x}), \ldots, \xi_k(\boldsymbol{x})]^{\mathrm{T}}$,where the $\xi_n(\boldsymbol{x})$ is the $n-$ th Gaussian basis function, $\boldsymbol{\mu}_n = [\mu_{n1}, \ldots \mu_{np}]^{\mathrm{T}}$ and λ_n are the center vector and the standard deviation, respectively. $\boldsymbol{\varepsilon}_w(\boldsymbol{x}) = [\varepsilon_{w1}(\boldsymbol{x}), \ldots, \varepsilon_{wq}(\boldsymbol{x})]^{\mathrm{T}}$ is the approximation error vector, and we assume that $\|\boldsymbol{\varepsilon}_w(\boldsymbol{x})\| \leq D_w, \forall \boldsymbol{x} \in \Re^p$, where D_w is an unknown positive constant. According to [32], there is an optimal NN weight matrix $\boldsymbol{W}^*$ that makes $\|\boldsymbol{\varepsilon}_w\|$ minimize for any $\boldsymbol{x} \in \Re^p$ such that

$$\begin{cases} \boldsymbol{f}(\boldsymbol{x}) = \boldsymbol{W}^*\boldsymbol{\xi}(\boldsymbol{x}) + \boldsymbol{\varepsilon}_w(\boldsymbol{x}), \quad \forall \boldsymbol{x} \in \Re^p \\ \boldsymbol{W}^* = \operatorname{argmin}\{\sup \|\boldsymbol{f}(\boldsymbol{x}) - \boldsymbol{W}\xi(\boldsymbol{x})\|\}, \\ \qquad\qquad \boldsymbol{W} \in \Re^{q\times k}, \quad \boldsymbol{x} \in \Re^p \end{cases} \tag{2}$$

where $\boldsymbol{W}^*$ is the ideal weight matrix, and $\varepsilon_w^*(x)$ is the approximation error for $\boldsymbol{W} \to \boldsymbol{W}^*$. However, the definition of $\boldsymbol{W}^*$ is very challenging. Therefore, an estimate of NN weights matrix $\hat{W}$ is introduced to approximate unknown function

as $\hat{\boldsymbol{f}}(\boldsymbol{x}) = \hat{\boldsymbol{W}}\xi(\boldsymbol{x})$, and the $\hat{\boldsymbol{W}}$ is usually estimated by an adaptive rule that is designed based on Lyapunov stability theory, and we assume that $\|\boldsymbol{W}\|_F \leq W_m$, where W_m is a positive unknown constant.

B. PROBLEM STATEMENT

1) MODEL OF AN UNDERACTUATED AUV

The dynamic model of AUV in the three-dimensional space is presented in this section. Ignore the effects of the AUV rolling, and the 5-degree-of-freedom dynamic model of the AUV can be considered as follows [33]:

The AUV kinematic equation is:

$$\begin{cases} \dot{x} = u\cos(\theta)\cos(\psi) - v\sin(\psi) + w\sin(\theta)\cos(\psi) \\ \dot{y} = u\cos(\theta)\sin(\psi) + v\cos(\psi) + w\sin(\theta)\sin(\psi) \\ \dot{z} = -u\sin(\theta) + w\cos(\theta) \\ \dot{\theta} = q \\ \dot{\psi} = r/\cos(\theta) \end{cases} \tag{3}$$

The AUV dynamic equation is:

$$\begin{cases} \dot{u} = \dfrac{m_{22}}{m_{11}}vr - \dfrac{m_{33}}{m_{11}}wq - f_u(u) + \dfrac{1}{m_{11}}\tau_u - \dfrac{1}{m_{11}}d_u(t) \\ \dot{v} = -\dfrac{m_{11}}{m_{22}}ur - f_v(v) - \dfrac{1}{m_{22}}d_v(t) \\ \dot{w} = \dfrac{m_{11}}{m_{33}}uq - f_w(w) - \dfrac{1}{m_{33}}d_w(t) \\ \dot{q} = \dfrac{m_{33} - m_{11}}{m_{55}}uw - f_q(q) - \dfrac{\rho g \nabla G M_L \sin(\theta)}{m_{55}} \\ \qquad + \dfrac{\tau_q}{m_{55}} - \dfrac{d_q(t)}{m_{55}} \\ \dot{r} = \dfrac{m_{11} - m_{22}}{m_{66}}uv - f_r(r) + \dfrac{1}{m_{66}}\tau_r - \dfrac{1}{m_{66}}d_r(t) \end{cases} \tag{4}$$

where x, y, z, θ and ψ represent positions and orientations of velocities in the earth fixed frame, respectively; u, v and w denote the surge, sway and heave velocities in the body fixed frame, respectively; q and r represent pitch angular velocity and yaw angular velocities, respectively; The signals τ_u, τ_q and τ_r represent control inputs that are provided by propellers and thrusters; $f_k(k), k = u, v, w, q, r$ represent the unknown nonlinear dynamics of AUV including friction terms and the hydrodynamic damping terms, and $d_k(t)$, $k = u, v, w, q, r$ represent bounded external environmental disturbances that are produced by the ocean currents, waves and wind, and $m_{ii}, i = 1, 2, 3, 5, 6$ represent the combined inertia and added mass terms; Other signals and parameters can be found in [34].

C. AUV PATH FOLLOWING ERROR DYNAMICS

The three-dimensional path following dynamic error model is proposed in this section. In Figure 2, l_d is the desired path described by design parameters.$\{E\}$, $\{B\}$ and $\{F\}$ denote the earth fixed frame, body fixed frame and Serret-Frenet frame respectively. Q denotes mass center of the AUV, which coincides with the origin of frame $\{B\}$, and P denotes the virtual reference guidance point in Serret-Frenet frame.

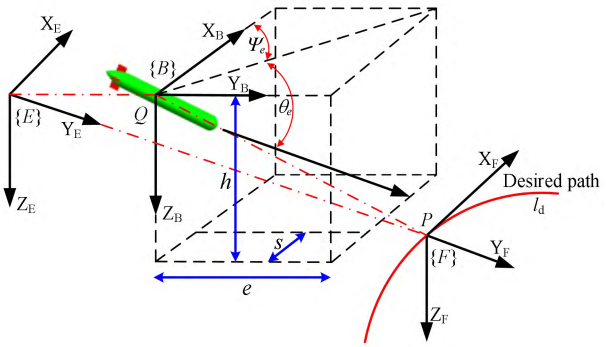

FIGURE 2. Diagram of three-dimensional path following of AUV.

Consider the course angle θ_F, ψ_F rotating around the axis Z_E and Y_E, respectively [35].

$$\begin{cases} \theta_F = -\arctan\left(\dfrac{\dot{z}_d(s)}{\sqrt{\dot{x}_d^2(s) + \dot{y}_d^2(s)}}\right) \\ \psi_F = \arctan\left(\dfrac{\dot{y}_d(s)}{\dot{x}_d(s)}\right) \end{cases} \tag{5}$$

where $\dot{x}_d = \frac{\partial x_d}{\partial s}, \dot{y}_d = \frac{\partial y_d}{\partial s}, \dot{z}_d = \frac{\partial z_d}{\partial s}$, and s is the parameter of desired path. We define the position of point P is $\boldsymbol{\eta}_d^n = [x_d(s), y_d(s), z_d(s)]^{\mathrm{T}}$, and the position of point Q in the earth fixed frame is $\boldsymbol{\eta}^n = [x, y, z]^{\mathrm{T}}$. The path following error can be defined as:

$$\boldsymbol{\varepsilon} = [s, e, h]^{\mathrm{T}} = \boldsymbol{R}_b^{n\mathrm{T}}(\boldsymbol{\eta}^n - \boldsymbol{\eta}_d^n) \tag{6}$$

where $\boldsymbol{R}_b^n$ is the rotation matrix from the frame $\{B\}$ to $\{E\}$, and differentiate $\boldsymbol{\varepsilon}$ with respect to time yields:

$$\dot{\boldsymbol{\varepsilon}} = \dot{\boldsymbol{R}}_b^{n\mathrm{T}}(\boldsymbol{\eta}^n - \boldsymbol{\eta}_d^n) + \boldsymbol{R}_b^{n\mathrm{T}}(\dot{\boldsymbol{\eta}}^n - \dot{\boldsymbol{\eta}}_d^n) \tag{7}$$

where $\dot{\boldsymbol{R}}_b^n = \boldsymbol{R}_b^n\boldsymbol{S}(\varpi_{qr})$, $\boldsymbol{S}(\varpi_{qr})$ denotes the angular velocity matrix.$\dot{\boldsymbol{\eta}}^n = \boldsymbol{R}_b^n\boldsymbol{v}_b$, $\boldsymbol{v}_b = [u, v, w]^{\mathrm{T}}$ is the velocities of AUV in the body fixed frame. $\dot{\boldsymbol{\eta}}_d^n = \boldsymbol{R}_F^n\boldsymbol{v}_F$, $\boldsymbol{R}_F^n$ is the rotation matrix from the frame $\{F\}$ to $\{E\}$, and $\boldsymbol{v}_F = [u_r, 0, 0]^{\mathrm{T}}$ is the virtual reference velocity.

$$\begin{aligned} \dot{\boldsymbol{\varepsilon}} &= \boldsymbol{S}^{\mathrm{T}}(\varpi_{qr})\boldsymbol{R}_b^{e\mathrm{T}}(\boldsymbol{\eta}^e - \boldsymbol{\eta}_d^e) + \boldsymbol{R}_b^{e\mathrm{T}}(\dot{\boldsymbol{\eta}}^e - \dot{\boldsymbol{\eta}}_d^e) \\ &= \boldsymbol{S}^{\mathrm{T}}(\varpi_{qr})\boldsymbol{\varepsilon} + \boldsymbol{R}_b^{e\mathrm{T}}\boldsymbol{R}_b^e\boldsymbol{v}_b - \boldsymbol{R}_b^{e\mathrm{T}}\boldsymbol{R}_F^e\boldsymbol{v}_F \\ &= \boldsymbol{S}^{\mathrm{T}}(\varpi_{qr})\boldsymbol{\varepsilon} + \boldsymbol{v}_b - \boldsymbol{R}(\psi_e, \theta_e)\boldsymbol{v}_F \end{aligned} \tag{8}$$

within

$$\boldsymbol{R}(\psi_e, \theta_e) = \begin{bmatrix} \cos\theta_e\cos\psi_e & -\sin\psi_e & \sin\theta_e\cos\psi_e \\ \cos\theta_e\sin\psi_e & \cos\psi_e & \sin\theta_e\sin\psi_e \\ -\sin\theta_e & 0 & \cos\theta_e \end{bmatrix} \tag{9}$$

and

$$\boldsymbol{S}(\varpi_{qr}) = \begin{bmatrix} 0 & r & -q \\ -r & 0 & 0 \\ q & 0 & 0 \end{bmatrix} \tag{10}$$

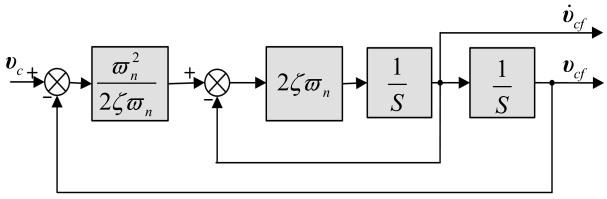

FIGURE 3. The structure of a second-order filter.

So the AUV path following error dynamics model in the three-dimensional space can be written as:

$$\begin{cases} \dot{s} = re - qh + u - u_r \cos\theta_e \cos\psi_e \\ \dot{e} = -rs + v - u_r \cos\theta_e \sin\psi_e \\ \dot{h} = qs + w + u_r \sin\theta_e \\ \dot{\theta}_e = q - \dot{\theta}_F \\ \dot{\psi}_e = r/\cos\theta - \dot{\psi}_F \end{cases} \tag{11}$$

where $\theta_e = \theta - \theta_F$, $\psi_e = \psi - \psi_F$, and $\theta \in (-\pi/2, \pi/2)$.

III. PATH FOLLOWING CONTROLLER DESIGN

A. POSITION CONTROL

According to (11), consider Lyapunov function V_1:

$$V_1 = \frac{1}{2}\left(s^2 + e^2 + h^2\right) \tag{12}$$

Differentiating V_1 along with (11) yields:

$$\begin{aligned} \dot{V}_1 = s\dot{s} + e\dot{e} + h\dot{h} &= s(u - u_r \cos\theta_e \cos\psi_e) \\ &+ h(w - u_r \sin\theta_e) + e(v + u_r \cos\theta_e \sin\psi_e) \end{aligned} \tag{13}$$

Define virtual control values u_c, θ_c and ψ_c, respectively:

$$\begin{cases} u_c = -\sigma_1 s + u_r \cos\theta_c \cos\psi_c \\ \theta_c = \arcsin\left(\sigma_2 h/\sqrt{1 + (\sigma_2 h)^2}\right) \\ \psi_c = -\arcsin\left(\sigma_3 e/\sqrt{1 + (\sigma_3 e)^2}\right) \end{cases} \tag{14}$$

where σ_1, σ_2 and σ_3 are unknown positive constants, and substitute (14) into (13) we get:

$$\begin{aligned} \dot{V}_1 = -\sigma_1 s^2 - \sigma_3 u_r \frac{1}{\sqrt{1 + (\sigma_2 h)^2}} \frac{e^2}{\sqrt{1 + (\sigma_3 e)^2}} \\ - \sigma_2 u_r \frac{h^2}{\sqrt{1 + (\sigma_2 h)^2}} + ev + hw \end{aligned} \tag{15}$$

In order to avoid the computational complexities of controller in traditional backstepping method, the virtual control values are passed by the command filter [36]. Then, a second-order filter is designed as follows:

$$\ddot{\boldsymbol{v}}_{cf} = -2\zeta\varpi_n \dot{\boldsymbol{v}}_{cf} - \varpi_n^2(\dot{\boldsymbol{v}}_{cf} - \boldsymbol{v}_c) \tag{16}$$

where $\boldsymbol{v}_c = [s_c, e_c, h_c, \theta_c, \psi_c, u_c, q_c, r_c]^{\mathrm{T}}$ is the vector of desired virtual control, and $\boldsymbol{v}_{cf} = [s_{cf}, e_{cf}, h_{cf}, \theta_{cf}, \psi_{cf}, u_{cf}, q_{cf}, r_{cf}]^{\mathrm{T}}$ is the filtered virtual control vector, ζ and ϖ_n are the unknown positive constants, where $0 < \zeta < 1$, and the structure of second-order filter is shown in Figure 3.

Define the filtered position tracking errors as:

$$\begin{cases} \tilde{s} = s - s_{cf} \\ \tilde{e} = e - e_{cf} \\ \tilde{h} = h - h_{cf} \end{cases} \tag{17}$$

Differentiating (17) along with (11) yields:

$$\begin{bmatrix} \dot{\tilde{s}} \\ \dot{\tilde{e}} \\ \dot{\tilde{h}} \end{bmatrix} = \begin{bmatrix} r\tilde{e} - q\tilde{h} \\ -r\tilde{s} \\ q\tilde{s} \end{bmatrix} + \left[\boldsymbol{A}\ \boldsymbol{B}f(\tilde{\psi})\ \boldsymbol{C}f(\tilde{\theta})\right] \begin{bmatrix} \tilde{u} \\ \tilde{\psi} \\ \tilde{\theta} \end{bmatrix} \tag{18}$$

where $\tilde{u} = u - u_{cf}$, $\tilde{\psi} = \psi_e - \psi_{cf}$, $\tilde{\theta} = \theta_e - \theta_{cf}$, $\boldsymbol{A} = [1, 0, 0]^{\mathrm{T}}$, and

$$\boldsymbol{B} = \begin{bmatrix} \cos\theta_e \cos\psi_{cf} & -\cos\theta_e \sin\psi_{cf} \\ \cos\theta_{cf} \sin\psi_{cf} & \cos\theta_{cf} \cos\psi_{cf} \\ 0 & 0 \end{bmatrix},$$

$$\boldsymbol{f}(\tilde{\theta}) = \begin{bmatrix} \dfrac{\cos\tilde{\theta} - 1}{\tilde{\theta}} \\ \dfrac{\sin\tilde{\theta}}{\tilde{\theta}} \end{bmatrix} u_r$$

$$\boldsymbol{C} = \begin{bmatrix} \cos\theta_{cf} \cos\psi_{cf} & -\cos\psi_{cf} \sin\theta_{cf} \\ \cos\psi_e \cos\theta_{cf} & -\sin\psi_e \sin\theta_{cf} \\ -\sin\theta_{cf} & -\cos\theta_{cf} \end{bmatrix},$$

$$\boldsymbol{f}(\tilde{\psi}) = \begin{bmatrix} \dfrac{\cos\tilde{\psi} - 1}{\tilde{\psi}} \\ \dfrac{\sin\tilde{\psi}}{\tilde{\psi}} \end{bmatrix} u_r$$

Conduct the following desired virtual control vector $[\dot{s}_c, \dot{e}_c, \dot{h}_c]^{\mathrm{T}}$ as:

$$\begin{cases} \dot{s}_c = \dot{s}_{cf} - \chi_s \tilde{s} \\ \dot{e}_c = \dot{e}_{cf} - \chi_e \tilde{e} \\ \dot{h}_c = \dot{h}_{cf} - \chi_h \tilde{h} \end{cases} \tag{19}$$

Substituting (19) into (18) yields:

$$\begin{aligned} \begin{bmatrix} \dot{\tilde{s}} \\ \dot{\tilde{e}} \\ \dot{\tilde{h}} \end{bmatrix} = \begin{bmatrix} r\tilde{e} - q\tilde{h} \\ -r\tilde{s} \\ q\tilde{s} \end{bmatrix} + \begin{bmatrix} \dot{s}_{cf} - \dot{s}_c \\ \dot{e}_{cf} - \dot{e}_c \\ \dot{h}_{cf} - \dot{h}_c \end{bmatrix} + \begin{bmatrix} -\chi_s \tilde{s} \\ -\chi_e \tilde{e} \\ -\chi_h \tilde{h} \end{bmatrix} \\ + \left[\boldsymbol{A}\ \boldsymbol{B}f(\tilde{\psi})\ \boldsymbol{C}f(\tilde{\theta})\right] \begin{bmatrix} \tilde{u} \\ \tilde{\psi} \\ \tilde{\theta} \end{bmatrix} \end{aligned} \tag{20}$$

B. ATTITUDE CONTROL

Defining $\tilde{\psi} = \psi_e - \psi_{cf}$, $\tilde{\theta} = \theta_e - \theta_{cf}$, and differentiating $\tilde{\psi}$ and $\tilde{\theta}$ yields:

$$\begin{cases} \dot{\tilde{\psi}} = r/\cos\theta - r_F - \dot{\psi}_{cf} \\ \quad = \dfrac{r_c + (r_{cf} - r_c) + \tilde{r}}{\cos\theta} - r_F - \dot{\psi}_{cf} \\ \dot{\tilde{\theta}} = q - q_F - \dot{\theta}_{cf} \\ \quad = q_c + (q_{cf} - q_c) + \tilde{q} - q_F - \dot{\theta}_{cf} \end{cases} \tag{21}$$

where $\tilde{r} = r - r_{cf}$, $\tilde{q} = q - q_{cf}$, and define the desired virtual control values r_c and q_c, respectively.

$$\begin{cases} r_c = (r_F + \dot{\psi}_{cf} - \chi_\psi \tilde{\psi} - \psi_{bs}) \cos\theta \\ q_c = q_F + \dot{\theta}_{cf} - \chi_\theta \tilde{\theta} - \theta_{bs} \end{cases} \tag{22}$$

where χ_ψ and χ_θ are unknown positive constants, ψ_{bs} and θ_{bs} are system robust terms which are designed in Section IV.

Substituting (22) into (21) yields:

$$\begin{cases} \dot{\tilde{\psi}} = \dfrac{r_c + (r_{cf} - r_c) + \tilde{r}}{\cos\theta} - \chi_\psi \tilde{\psi} - \psi_{bs} \\ \dot{\tilde{\theta}} = (q_{cf} - q_c) + \tilde{q} - \chi_\theta \tilde{\theta} - \theta_{bs} \end{cases} \tag{23}$$

C. VELOCITY AND ANGULAR VELOCITY CONTROL

Defining $\dot{\tilde{u}} = \dot{u} - \dot{u}_{cf}$, $\dot{\tilde{q}} = \dot{q} - \dot{q}_{cf}$ and $\dot{\tilde{r}} = \dot{r} - \dot{r}_{cf}$, and the follow-ing error equations are obtained:

$$\begin{cases} m_{11}\dot{\tilde{u}} = m_{22}vr - m_{33}wq - m_{11}f_u(u) - m_{11}\dot{u}_{cf} + \tau_u - d_u(t) \\ m_{55}\dot{\tilde{q}} = (m_{33} - m_{11})uw - m_{55}f_q(q) - \rho g \nabla G M_L \sin\theta \\ \qquad - m_{55}\dot{q}_{cf} + \tau_q - d_q(t) \\ m_{66}\dot{\tilde{r}} = (m_{11} - m_{22})uv - m_{66}f_r(r) - m_{66}\dot{r}_{cf} + \tau_r - d_r(t) \end{cases} \tag{24}$$

Then, the following controller in the surge direction is designed:

$$\begin{cases} \tau_u = -m_{11}(\chi_u \tilde{u} + \chi_{iu}\varepsilon_u + u_{bs}) \\ \qquad + \hat{\boldsymbol{W}}_u \boldsymbol{\xi}(\boldsymbol{x}_u) - \hat{\eta}_u \tanh(\nu \hat{\eta}_u \tilde{u}/\mu_u) \\ \dot{\hat{\boldsymbol{W}}}_u = -\lambda_{wu}\tilde{u}\boldsymbol{\xi}^{\mathrm{T}}(\boldsymbol{x}_u) - \lambda_{wu}\delta_u \hat{\boldsymbol{W}}_u \\ \dot{\hat{\eta}}_u = \lambda_{\eta u}|\tilde{u}| - \lambda_{\eta u}\kappa_u(\hat{\eta}_u - \eta_{u0}) \end{cases} \tag{25}$$

where $\chi_u, \chi_{iu}, \mu_u, \lambda_{wu}, \delta_u, \lambda_{\eta u}, \kappa_u, \eta_{u0}$ are the positive design parameters, ν satisfies $\nu = e^{-(\nu+1)}$, and $\boldsymbol{x}_u = [u, v, w, q, r, \dot{u}_{cf}]^{\mathrm{T}}$, $\dot{\varepsilon}_u = \tilde{u}$, and define $\varpi_u = \hat{\boldsymbol{W}}_u \boldsymbol{\xi}(\boldsymbol{x}_u) - \hat{\eta}_u \tanh(\nu \hat{\eta}_u \tilde{u}/\mu_u)$.

The following controller in pitch direction is presented:

$$\begin{cases} \tau_q = -m_{55}(\chi_q \tilde{q} + \chi_{iq}\varepsilon_q + q_{bs}) \\ \qquad + \hat{\boldsymbol{W}}_q \boldsymbol{\xi}(\boldsymbol{x}_q) - \hat{\eta}_q \tanh(\nu \hat{\eta}_q \tilde{q}/\mu_q) \\ \dot{\hat{\boldsymbol{W}}}_q = -\lambda_{wq}\tilde{q}\boldsymbol{\xi}^{\mathrm{T}}(\boldsymbol{x}_q) - \lambda_{wq}\delta_q \hat{\boldsymbol{W}}_q \\ \dot{\hat{\eta}}_q = \lambda_{\eta q}|\tilde{q}| - \lambda_{\eta q}\kappa_q(\hat{\eta}_q - \eta_{q0}) \end{cases} \tag{26}$$

where $\chi_q, \chi_{iq}, \mu_q, \lambda_{wq}, \delta_q, \lambda_{\eta q}, \kappa_q, \eta_{q0} > 0$ and $\boldsymbol{x}_q = [u, w, q, \theta, \dot{q}_{cf}]^{\mathrm{T}}$, $\dot{\varepsilon}_q = \tilde{q}$, and define $\varpi_q = \hat{\boldsymbol{W}}_q \boldsymbol{\xi}(\boldsymbol{x}_q) - \hat{\eta}_q \tanh(\nu \hat{\eta}_q \tilde{q}/\mu_q)$.

The following controller in the yaw direction is proposed

$$\begin{cases} \tau_r = -m_{66}(\chi_r \tilde{r} + \chi_{ir}\varepsilon_r + r_{bs}) \\ \qquad + \hat{\boldsymbol{W}}_r \boldsymbol{\xi}(\boldsymbol{x}_r) - \hat{\eta}_r \tanh(\nu \hat{\eta}_r \tilde{r}/\mu_r) \\ \dot{\hat{\boldsymbol{W}}}_r = -\lambda_{wr}\tilde{r}\boldsymbol{\xi}^{\mathrm{T}}(\boldsymbol{x}_r) - \lambda_{wr}\delta_r \hat{\boldsymbol{W}}_r \\ \dot{\hat{\eta}}_r = \lambda_{\eta r}|\tilde{r}| - \lambda_{\eta r}\kappa_r(\hat{\eta}_r - \eta_{r0}) \end{cases} \tag{27}$$

where $\chi_r, \chi_{ir}, \mu_r, \lambda_{wr}, \delta_r, \lambda_{\eta r}, \kappa_r, \eta_{r0} > 0$ and $\boldsymbol{x}_r = [u, v, r, \dot{r}_{cf}]^{\mathrm{T}}$, $\dot{\varepsilon}_r = \tilde{r}$, and define $\varpi_r = \hat{\boldsymbol{W}}_r \boldsymbol{\xi}(\boldsymbol{x}_r) - \hat{\eta}_r \tanh(\nu \hat{\eta}_r \tilde{r}/\mu_r)$, u_{bs}, q_{bs}, r_{bs} are the system robust terms that are designed in Section IV.

Then, substituting (25), (26) and (27) into (4) and the following error dynamics is proposed:

$$\begin{cases} m_{11}\dot{\tilde{u}} = -m_{11}(\chi_u \tilde{u} + \chi_{iu}\varepsilon_u + u_{bs}) + \varpi_u - \zeta_u - d_u(t) \\ m_{55}\dot{\tilde{q}} = -m_{55}(\chi_q \tilde{q} + \chi_{iq}\varepsilon_q + q_{bs}) + \varpi_q - \zeta_q - d_q(t) \\ m_{66}\dot{\tilde{r}} = -m_{66}(\chi_r \tilde{r} + \chi_{ir}\varepsilon_r + r_{bs}) + \varpi_r - \zeta_r - d_r(t) \end{cases} \tag{28}$$

where $\zeta_k = \boldsymbol{W}_k^* \boldsymbol{\xi}(\boldsymbol{x}_k) + \boldsymbol{\varepsilon}_{wk}, k = u, q, r$ are defined as follows:

$$\begin{cases} \zeta_u = -m_{22}vr + m_{33}wq + m_{11}f_u(u) + m_{11}\dot{u}_{cf} \\ \zeta_q = -(m_{33} - m_{11})uw + m_{55}f_q(q) \\ \qquad + \rho g \nabla G M_L \sin\theta + m_{55}\dot{q}_{cf} \\ \zeta_r = -(m_{11} - m_{22})uv + m_{66}f_r(r) + m_{66}\dot{r}_{cf} \end{cases} \tag{29}$$

Define $\dot{\varepsilon}_u = \tilde{u}$, $\dot{\varepsilon}_q = \tilde{q}$, $\dot{\varepsilon}_r = \tilde{r}$,and (28) can be written as:

$$\begin{cases} m_{11}\ddot{\varepsilon}_u = -m_{11}(\chi_u \dot{\varepsilon}_u + \chi_{iu}\varepsilon_u + u_{bs}) + \varpi_u - \zeta_u - d_u(t) \\ m_{55}\ddot{\varepsilon}_q = -m_{55}(\chi_q \dot{\varepsilon}_q + \chi_{iq}\varepsilon_q + q_{bs}) + \varpi_q - \zeta_q - d_q(t) \\ m_{66}\ddot{\varepsilon}_r = -m_{66}(\chi_r \dot{\varepsilon}_r + \chi_{ir}\varepsilon_r + r_{bs}) + \varpi_r - \zeta_r - d_r(t) \end{cases} \tag{30}$$

Then, define error vectors $\boldsymbol{\varepsilon} = [\varepsilon_u, \varepsilon_q, \varepsilon_r]^{\mathrm{T}}$, $\dot{\boldsymbol{\varepsilon}} = [\dot{\varepsilon}_u, \dot{\varepsilon}_q, \dot{\varepsilon}_r]^{\mathrm{T}}$ and $\boldsymbol{E} = [\boldsymbol{\varepsilon}^{\mathrm{T}}, \dot{\boldsymbol{\varepsilon}}^{\mathrm{T}}]^{\mathrm{T}}$, respectively, and (30) is finally rewritten as $\dot{\boldsymbol{E}} = \boldsymbol{M}\boldsymbol{E} + \boldsymbol{N}\boldsymbol{U}$, where:

$$\boldsymbol{M} = \begin{bmatrix} 0_{3\times3} & \boldsymbol{I}_{3\times3} \\ -\boldsymbol{K}_{I3\times3} & -\boldsymbol{K}_{P3\times3} \end{bmatrix} \boldsymbol{N} = \begin{bmatrix} 0_{3\times3} \\ \boldsymbol{I}_{3\times3} \end{bmatrix}$$

$$\boldsymbol{U} = \begin{bmatrix} -u_{bs} + m_{11}^{-1}[\varpi_u - \zeta_u - d_u(t)] \\ -q_{bs} + m_{55}^{-1}[\varpi_q - \zeta_q - d_q(t)] \\ -r_{bs} + m_{66}^{-1}[\varpi_r - \zeta_r - d_r(t)] \end{bmatrix}$$

$$\boldsymbol{K}_{P3\times3} = diag\{-\chi_u, -\chi_q, -\chi_r\},$$

$$\boldsymbol{K}_{I3\times3} = diag\{-\chi_{iu}, -\chi_{iq}, -\chi_{ir}\}$$

D. FILTER ERROR COMPENSATION LOOP DESIGN

To guarantee the approximation precision between the command virtual control and the filtered signal, a filtered error compensation loop is developed in this section.

Define position filtered compensation errors $\vartheta_s = \tilde{s} - \alpha_s$, $\vartheta_e = \tilde{e} - \alpha_e$, $\vartheta_h = \tilde{h} - \alpha_h$, where $\alpha_s, \alpha_e, \alpha_h$ are constructed as:

$$\begin{bmatrix} \dot{\alpha}_s \\ \dot{\alpha}_e \\ \dot{\alpha}_h \end{bmatrix} = \begin{bmatrix} r\alpha_e - q\alpha_h \\ -r\alpha_s \\ q\alpha_s \end{bmatrix} + \begin{bmatrix} \dot{s}_{cf} - \dot{s}_c \\ \dot{e}_{cf} - \dot{e}_c \\ \dot{h}_{cf} - \dot{h}_c \end{bmatrix} + \begin{bmatrix} -\chi_s\alpha_s \\ -\chi_e\alpha_e \\ -\chi_h\alpha_h \end{bmatrix} + \left[\boldsymbol{A}\ \boldsymbol{B}f(\tilde{\psi})\ \boldsymbol{C}f(\tilde{\theta})\right] \begin{bmatrix} \alpha_u \\ \alpha_\psi \\ \alpha_\theta \end{bmatrix} \tag{31}$$

where $\alpha_s(0) = 0, \alpha_e(0) = 0, \alpha_h(0) = 0$; $\alpha_\psi, \alpha_\theta$ are defined in (35), and then consider a Lyapunov function as:

$$V_1 = \frac{1}{2}(\vartheta_s^2 + \vartheta_e^2 + \vartheta_h^2) \tag{32}$$

Differentiating (32) along with (20) and (31) yields:

$$\begin{aligned} \dot{V}_1 &= \vartheta_s\dot{\vartheta}_s + \vartheta_e\dot{\vartheta}_e + \vartheta_h\dot{\vartheta}_h = -\chi_s\vartheta_s^2 - \chi_e\vartheta_e^2 - \chi_h\vartheta_h^2 \\ &\quad + [\vartheta_s, \vartheta_e, \vartheta_h] \times \left[\boldsymbol{A}\ \boldsymbol{Bf}(\tilde{\psi})\ \boldsymbol{Cf}(\tilde{\theta})\right] \times \begin{bmatrix} \alpha_u \\ \alpha_\psi \\ \alpha_\theta \end{bmatrix} \\ &= -\chi_s\vartheta_s^2 - \chi_e\vartheta_e^2 - \chi_h\vartheta_h^2 + \boldsymbol{A}^{\mathrm{T}}[\vartheta_s, \vartheta_e, \vartheta_h]^{\mathrm{T}}\vartheta_u \\ &\quad + \boldsymbol{f}^{\mathrm{T}}(\tilde{\psi})\boldsymbol{B}^{\mathrm{T}} \begin{bmatrix} \vartheta_s \\ \vartheta_e \\ \vartheta_h \end{bmatrix} \vartheta_\psi + \boldsymbol{f}^{\mathrm{T}}(\tilde{\theta})\boldsymbol{C}^{\mathrm{T}} \begin{bmatrix} \vartheta_s \\ \vartheta_e \\ \vartheta_h \end{bmatrix} \vartheta_\theta \end{aligned} \tag{33}$$

where $\vartheta_u = \tilde{u} = u - u_{cf}$, $\vartheta_\psi, \vartheta_\theta$ are defined in (34).

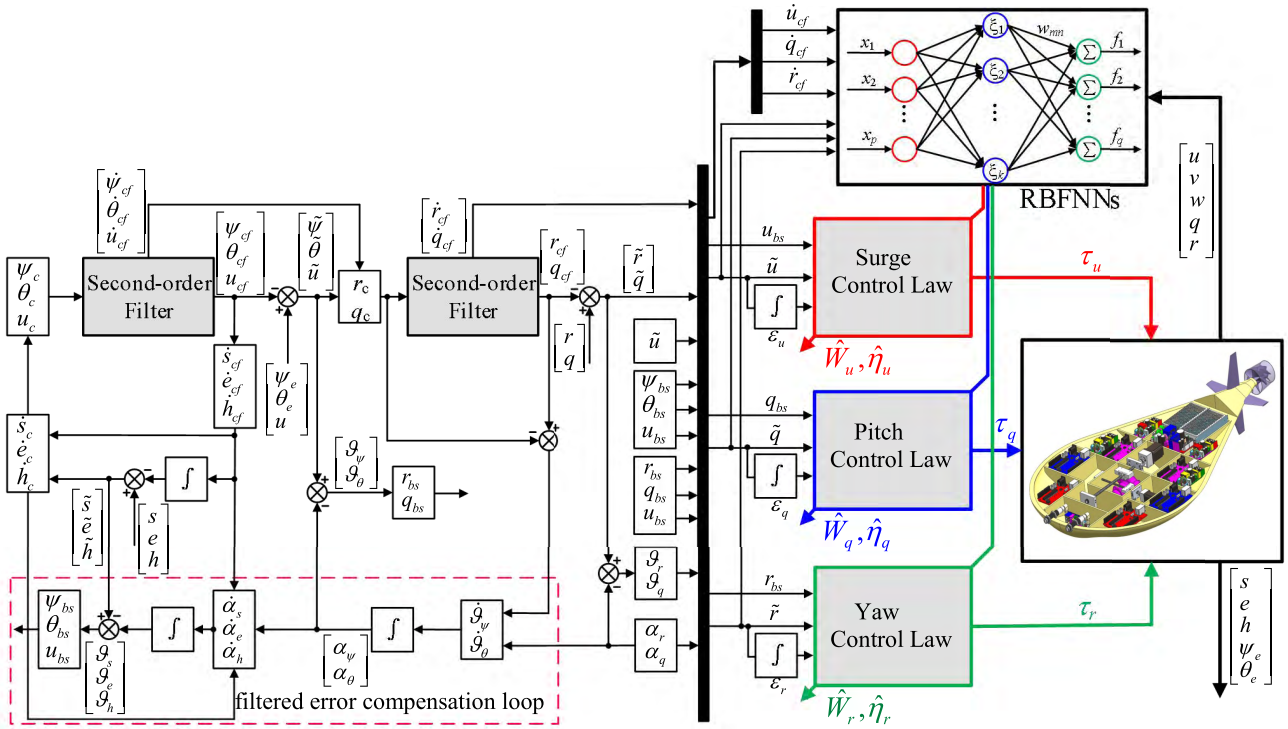

FIGURE 4. Block diagram of the proposed path following control system.

Define the attitude filtered compensation errors as:

$$\begin{cases} \vartheta_\psi = \tilde{\psi} - \alpha_\psi \\ \vartheta_\theta = \tilde{\theta} - \alpha_\theta \end{cases} \tag{34}$$

According to (23), α_ψ, α_θ can be constructed as:

$$\begin{cases} \dot{\alpha}_\psi = \dfrac{(r_{cf} - r_c)}{\cos\theta} + \dfrac{\alpha_r}{\cos\theta} - \chi_\psi \alpha_\psi \\ \dot{\alpha}_\theta = (q_{cf} - q_c) + \alpha_q - \chi_\theta \alpha_\theta \end{cases} \tag{35}$$

where $\alpha_\psi(0) = 0, \alpha_\theta(0) = 0, \alpha_r = 0, \alpha_q = 0$.

Then, consider a new Lyapunov function as:

$$V_2 = \frac{1}{2}(\vartheta_\psi^2 + \vartheta_\theta^2) \tag{36}$$

Differentiating (36) along with (23) and (35) yields:

$$\begin{aligned} \dot{V}_2 &= \vartheta_\psi \dot{\vartheta}_\psi + \vartheta_\theta \dot{\vartheta}_\theta \\ &= \left(\dot{\tilde{\psi}} - \dot{\alpha}_\psi\right)\vartheta_\psi + \left(\dot{\tilde{\theta}} - \dot{\alpha}_\theta\right)\vartheta_\theta \\ &= \left(\frac{\tilde{r}}{\cos\theta} - \chi_\psi \tilde{\psi} - \psi_{bs} + \chi_\psi \alpha_\psi - \frac{\alpha_r}{\cos\theta}\right)\vartheta_\psi \\ &\quad + \left(-\chi_\theta \tilde{\theta} + \tilde{q} - \theta_{bs} + \chi_\theta \alpha_\theta - \alpha_q\right)\vartheta_\theta \\ &= -\chi_\psi \vartheta_\psi^2 - \chi_\theta \vartheta_\theta^2 + \frac{\vartheta_r}{\cos\theta}\vartheta_\psi + \vartheta_q \vartheta_\theta - \theta_{bs}\vartheta_\theta - \psi_{bs}\vartheta_\psi \end{aligned} \tag{37}$$

where $\vartheta_q = \tilde{q} = q - q_{cf}$ and $\vartheta_r = \tilde{r} = r - r_{cf}$.

Figure 4 illustrates a block diagram of the proposed path following control system. In the next section, the stability analysis of the closed-loop control system is proposed.

IV. STABILITY ANALYSIS

Theorem 1: Consider the three-dimensional path following error system of the underactuated AUVs which is denoted by (11). The neuro-adaptive command filtered backstepping controller (25), (26) and (27) combined with the robust compensation term (40) and (41), guarantees that all the signals in the closed-loop control system are bounded, and the path following errors uniformly ultimately converge to a small neighborhood of the zero.

Proof: Consider the following Lyapunov function for the overall closed-loop system:

$$\begin{aligned} V_3 &= V_1 + V_2 + \frac{1}{2}\boldsymbol{E}^{\mathrm{T}}\boldsymbol{P}\boldsymbol{E} \\ &\quad + \frac{1}{2}\left(\frac{p_{21}\tilde{\boldsymbol{W}}_u^{\mathrm{T}}\tilde{\boldsymbol{W}}_u}{m_{11}\lambda_{wu}} + \frac{p_{22}\tilde{\boldsymbol{W}}_q^{\mathrm{T}}\tilde{\boldsymbol{W}}_q}{m_{55}\lambda_{wq}} + \frac{p_{23}\tilde{\boldsymbol{W}}_r^{\mathrm{T}}\tilde{\boldsymbol{W}}_r}{m_{66}\lambda_{wr}}\right. \\ &\quad \left. + \frac{p_{21}\tilde{\eta}_u^2}{m_{11}\lambda_{\eta u}} + \frac{p_{22}\tilde{\eta}_q^2}{m_{55}\lambda_{\eta q}} + \frac{p_{23}\tilde{\eta}_r^2}{m_{66}\lambda_{\eta r}}\right) \\ &= \frac{1}{2}(\vartheta_s^2 + \vartheta_e^2 + \vartheta_h^2 + \vartheta_\psi^2 + \vartheta_\theta^2 + \boldsymbol{E}^{\mathrm{T}}\boldsymbol{P}\boldsymbol{E}) \\ &\quad + \frac{1}{2}\left(\frac{p_{21}\tilde{\boldsymbol{W}}_u^{\mathrm{T}}\tilde{\boldsymbol{W}}_u}{m_{11}\lambda_{wu}} + \frac{p_{22}\tilde{\boldsymbol{W}}_q^{\mathrm{T}}\tilde{\boldsymbol{W}}_q}{m_{55}\lambda_{wq}} + \frac{p_{23}\tilde{\boldsymbol{W}}_r^{\mathrm{T}}\tilde{\boldsymbol{W}}_r}{m_{66}\lambda_{wr}}\right. \\ &\quad \left. + \frac{p_{21}\tilde{\eta}_u^2}{m_{11}\lambda_{\eta u}} + \frac{p_{22}\tilde{\eta}_q^2}{m_{55}\lambda_{\eta q}} + \frac{p_{23}\tilde{\eta}_r^2}{m_{66}\lambda_{\eta r}}\right) \end{aligned} \tag{38}$$

where $\boldsymbol{P} = \begin{bmatrix} \boldsymbol{P}_1 & 0_{3\times3} \\ 0_{3\times3} & \boldsymbol{P}_2 \end{bmatrix}$ is a positive definite symmetric matrix, $\boldsymbol{P}_i = diag\{p_{i1}, p_{i2}, p_{i3}\}, i = 1, 2$, and $\tilde{\boldsymbol{W}}_k = \boldsymbol{W}_k^* - \hat{\boldsymbol{W}}_k, \tilde{\eta}_k = \eta_k^* - \hat{\eta}_k, k = u, q, r$.

Then, define $\boldsymbol{M}^{\mathrm{T}}\boldsymbol{P} + \boldsymbol{M}\boldsymbol{A} = -2\boldsymbol{Q}$ and differentiate (38) along with (30), (33) and (37) yields:

$$\begin{aligned}
\dot{V}_3 = {} & \dot{V}_1 + \dot{V}_2 + \boldsymbol{E}^{\mathrm{T}}\boldsymbol{P}\dot{\boldsymbol{E}} - \frac{p_{21}\tilde{\boldsymbol{W}}_u^{\mathrm{T}}\dot{\hat{\boldsymbol{W}}}_u}{m_{11}\lambda_{wu}} \\
& - \frac{p_{22}\tilde{\boldsymbol{W}}_q^{\mathrm{T}}\dot{\hat{\boldsymbol{W}}}_q}{m_{55}\lambda_{wq}} - \frac{p_{23}\tilde{\boldsymbol{W}}_r^{\mathrm{T}}\dot{\hat{\boldsymbol{W}}}_r}{m_{66}\lambda_{wr}} \\
& - \frac{p_{21}\tilde{\eta}_u\dot{\hat{\eta}}_u}{m_{11}\lambda_{\eta u}} - \frac{p_{22}\tilde{\eta}_q\dot{\hat{\eta}}_q}{m_{55}\lambda_{\eta q}} - \frac{p_{23}\tilde{\eta}_r\dot{\hat{\eta}}_r}{m_{66}\lambda_{\eta r}} \\
= {} & -\chi_s\vartheta_s^2 - \chi_e\vartheta_e^2 - \chi_h\vartheta_h^2 - \chi_\psi\vartheta_\psi^2 - \chi_\theta\vartheta_\theta^2 - \boldsymbol{E}^{\mathrm{T}}\boldsymbol{Q}\boldsymbol{E} \\
& + \boldsymbol{A}^{\mathrm{T}}\begin{bmatrix}\vartheta_s\\ \vartheta_e\\ \vartheta_h\end{bmatrix}\vartheta_u + \boldsymbol{f}^{\mathrm{T}}(\tilde{\psi})\boldsymbol{B}^{\mathrm{T}}\begin{bmatrix}\vartheta_s\\ \vartheta_e\\ \vartheta_h\end{bmatrix}\vartheta_\psi \\
& + \boldsymbol{f}^{\mathrm{T}}(\tilde{\theta})\boldsymbol{C}^{\mathrm{T}}\begin{bmatrix}\vartheta_s\\ \vartheta_e\\ \vartheta_h\end{bmatrix}\vartheta_\theta \\
& + \frac{\vartheta_r}{\cos\theta}\vartheta_\psi + \vartheta_q\vartheta_\theta - \theta_{bs}\vartheta_\theta - \psi_{bs}\vartheta_\psi \\
& - p_{21}\vartheta_u u_{bs} - p_{22}\vartheta_q q_{bs} \\
& - p_{23}\vartheta_r r_{bs} - p_{21}m_{11}^{-1}\vartheta_u \\
& \times \left(\tilde{\boldsymbol{W}}_u\boldsymbol{\xi}(\boldsymbol{x}_u) + \hat{\eta}_u\tanh(\nu\hat{\eta}_u\tilde{u}/\mu_u) + \varepsilon_{wu}\right. \\
& + \left. d_u(t)\right) - p_{22}m_{55}^{-1}\vartheta_q \\
& \times \left(\tilde{\boldsymbol{W}}_q\boldsymbol{\xi}(\boldsymbol{x}_q) + \hat{\eta}_q\tanh(\nu\hat{\eta}_q\tilde{q}/\mu_q) + \varepsilon_{wq}\right. \\
& + \left. d_q(t)\right) - p_{23}m_{66}^{-1}\vartheta_r \\
& \times \left(\tilde{\boldsymbol{W}}_r\boldsymbol{\xi}(\boldsymbol{x}_r) + \hat{\eta}_r\tanh(\nu\hat{\eta}_r\tilde{r}/\mu_r) + \varepsilon_{wr}\right. \\
& + \left. d_r(t)\right) - \frac{p_{21}\tilde{\boldsymbol{W}}_u^{\mathrm{T}}\dot{\hat{\boldsymbol{W}}}_u}{m_{11}\lambda_{wu}} - \frac{p_{22}\tilde{\boldsymbol{W}}_q^{\mathrm{T}}\dot{\hat{\boldsymbol{W}}}_q}{m_{55}\lambda_{wq}} \\
& - \frac{p_{23}\tilde{\boldsymbol{W}}_r^{\mathrm{T}}\dot{\hat{\boldsymbol{W}}}_r}{m_{66}\lambda_{wr}} - \frac{p_{21}\tilde{\eta}_u\dot{\hat{\eta}}_u}{m_{11}\lambda_{\eta u}} \\
& - \frac{p_{22}\tilde{\eta}_q\dot{\hat{\eta}}_q}{m_{55}\lambda_{\eta q}} - \frac{p_{23}\tilde{\eta}_r\dot{\hat{\eta}}_r}{m_{66}\lambda_{\eta r}}
\end{aligned} \tag{39}$$

where $\boldsymbol{Q} = \frac{1}{2}\begin{bmatrix} 0_{3\times3} & \boldsymbol{K}_I\boldsymbol{P}_2 - \boldsymbol{P}_1 \\ \boldsymbol{K}_I\boldsymbol{P}_2 - \boldsymbol{P}_1 & 2\boldsymbol{K}_I\boldsymbol{P}_2 \end{bmatrix} = \begin{bmatrix} 0_{3\times3} & 0_{3\times3} \\ 0_{3\times3} & \boldsymbol{K}_I\boldsymbol{P}_2 \end{bmatrix}$ with choosing $\boldsymbol{P}_1 = \boldsymbol{K}_I\boldsymbol{P}_2$.

Then, choose the following system robust terms:

$$\psi_{bs} = \boldsymbol{f}^{\mathrm{T}}(\tilde{\psi})\boldsymbol{B}^{\mathrm{T}}\begin{bmatrix}\vartheta_s\\ \vartheta_e\\ \vartheta_h\end{bmatrix}, \quad \theta_{bs} = \boldsymbol{f}^{\mathrm{T}}(\tilde{\theta})\boldsymbol{C}^{\mathrm{T}}\begin{bmatrix}\vartheta_s\\ \vartheta_e\\ \vartheta_h\end{bmatrix},$$
$$u_{bs} = \frac{1}{p_{21}}\boldsymbol{A}^{\mathrm{T}}\begin{bmatrix}\vartheta_s\\ \vartheta_e\\ \vartheta_h\end{bmatrix} \tag{40}$$
$$r_{bs} = \frac{\vartheta_\psi}{p_{23}\cos\theta}, \quad q_{bs} = \frac{\vartheta_\theta}{p_{22}} \tag{41}$$

Substituting (40) and (41) into (39) yields:

$$\begin{aligned}
\dot{V}_3 = {} & -\chi_s\vartheta_s^2 - \chi_e\vartheta_e^2 - \chi_h\vartheta_h^2 - \chi_\psi\vartheta_\psi^2 - \chi_\theta\vartheta_\theta^2 - \boldsymbol{E}^{\mathrm{T}}\boldsymbol{Q}\boldsymbol{E} \\
& - p_{21}m_{11}^{-1}\vartheta_u\left(\tilde{\boldsymbol{W}}_u\boldsymbol{\xi}(\boldsymbol{x}_u) + \hat{\eta}_u\tanh(\nu\hat{\eta}_u\tilde{u}/\mu_u) + \varepsilon_{wu} + d_u(t)\right) \\
& - p_{22}m_{55}^{-1}\vartheta_q\left(\tilde{\boldsymbol{W}}_q\boldsymbol{\xi}(\boldsymbol{x}_q) + \hat{\eta}_q\tanh(\nu\hat{\eta}_q\tilde{q}/\mu_q) + \varepsilon_{wq} + d_q(t)\right) \\
& - p_{23}m_{66}^{-1}\vartheta_r\left(\tilde{\boldsymbol{W}}_r\boldsymbol{\xi}(\boldsymbol{x}_r) + \hat{\eta}_r\tanh(\nu\hat{\eta}_r\tilde{r}/\mu_r) + \varepsilon_{wr} + d_r(t)\right) \\
& - \frac{p_{21}\tilde{\boldsymbol{W}}_u^{\mathrm{T}}\dot{\hat{\boldsymbol{W}}}_u}{m_{11}\lambda_{wu}} - \frac{p_{22}\tilde{\boldsymbol{W}}_q^{\mathrm{T}}\dot{\hat{\boldsymbol{W}}}_q}{m_{55}\lambda_{wq}} - \frac{p_{23}\tilde{\boldsymbol{W}}_r^{\mathrm{T}}\dot{\hat{\boldsymbol{W}}}_r}{m_{66}\lambda_{wr}} - \frac{p_{21}\tilde{\eta}_u\dot{\hat{\eta}}_u}{m_{11}\lambda_{\eta u}} \\
& - \frac{p_{22}\tilde{\eta}_q\dot{\hat{\eta}}_q}{m_{55}\lambda_{\eta q}} - \frac{p_{23}\tilde{\eta}_r\dot{\hat{\eta}}_r}{m_{66}\lambda_{\eta r}}
\end{aligned} \tag{42}$$

Then, the equation (42) is expressed as follows by considering, $|\varepsilon_{wk} + d_k| \le \eta_k, \tilde{\boldsymbol{W}}_k^{\mathrm{T}}\hat{\boldsymbol{W}}_k \le -\alpha_1\left\|\tilde{\boldsymbol{W}}_k\right\|_F^2 + \alpha_2\left\|\boldsymbol{W}_k^*\right\|_F^2$, and $\tilde{\eta}_k(\hat{\eta}_k - \eta_{k0}) \le -\alpha_1|\tilde{\eta}_k|^2 + \alpha_2\left|\eta_k^* - \eta_{k0}\right|^2$, $k = u, q, r$, with $\alpha_1 = 1 - 0.5/\kappa^2, \alpha_2 = 0.5/\kappa^2$ and $\kappa > \sqrt{2}/2$, and combining with (25), (26) and (27):

$$\begin{aligned}
\dot{V}_3 \le {} & -\chi_s\vartheta_s^2 - \chi_e\vartheta_e^2 - \chi_h\vartheta_h^2 - \chi_\psi\vartheta_\psi^2 - \chi_\theta\vartheta_\theta^2 - \boldsymbol{E}^{\mathrm{T}}\boldsymbol{Q}\boldsymbol{E} \\
& - \alpha_1\delta_u p_{21}m_{11}^{-1}\left\|\tilde{\boldsymbol{W}}_u\right\|_F^2 - \alpha_1\delta_q p_{22}m_{55}^{-1}\left\|\tilde{\boldsymbol{W}}_q\right\|_F^2 \\
& - \alpha_1\delta_r p_{23}m_{66}^{-1}\left\|\tilde{\boldsymbol{W}}_r\right\|_F^2 \\
& - \alpha_1\kappa_u p_{21}m_{11}^{-1}|\tilde{\eta}_u|^2 - \alpha_1\kappa_q p_{22}m_{55}^{-1}|\tilde{\eta}_q|^2 \\
& - \alpha_1\kappa_r p_{23}m_{66}^{-1}|\tilde{\eta}_r|^2 \\
& + \alpha_2\delta_u p_{21}m_{11}^{-1}\left\|\boldsymbol{W}_u^*\right\|_F^2 \\
& + \alpha_2\delta_q p_{22}m_{55}^{-1}\left\|\boldsymbol{W}_q^*\right\|_F^2 + \alpha_2\delta_r p_{23}m_{66}^{-1}\left\|\boldsymbol{W}_r^*\right\|_F^2 \\
& + \alpha_2\kappa_u p_{21}m_{11}^{-1}\left|\eta_u^* - \eta_{u0}\right|^2 + \alpha_2\kappa_q p_{22}m_{55}^{-1}\left|\eta_q^* - \eta_{q0}\right|^2 \\
& + \alpha_2\kappa_r p_{23}m_{66}^{-1}\left|\eta_r^* - \eta_{r0}\right|^2 + \mu_u + \mu_q + \mu_r
\end{aligned} \tag{43}$$

Then, (43) finally results in the following differential inequality:

$$\dot{V}_3(t) \le -(\rho_{\min}/\rho_{\max})V_3(t) + \mu \tag{44}$$

where: $\rho_{\max} = \max\{1, \rho_P, \frac{p_{21}}{m_{11}\lambda_{wu}}, \frac{p_{22}}{m_{55}\lambda_{wq}}, \frac{p_{23}}{m_{66}\lambda_{wr}}, \frac{p_{21}}{m_{11}\eta_{wu}}, \frac{p_{22}}{m_{55}\eta_{wq}}, \frac{p_{23}}{m_{66}\eta_{wr}}\}\rho_{\min} = \min\{\chi_s, \chi_e, \chi_h, \chi_\psi, \chi_\theta, \rho_Q, \rho_{wu}, \rho_{wq}, \rho_{wr}, \rho_{\eta u}, \rho_{\eta q}, \rho_{\eta r}\}$, and $\rho_{wu} = \alpha_1\delta_u p_{21}m_{11}^{-1}, \rho_{wq} = \alpha_1\delta_q p_{22}m_{55}^{-1}, \rho_{wr} = \alpha_1\delta_r p_{23}m_{66}^{-1}, \rho_{\eta u} = \alpha_1\kappa_u p_{21}m_{11}^{-1}, \rho_{\eta q} = \alpha_1\kappa_q p_{22}m_{55}^{-1}, \rho_{\eta r} = \alpha_1\kappa_r p_{23}m_{66}^{-1}$, and ρ_P is the maximum value in the matrix $\boldsymbol{P}$, ρ_Q is the minimum value in the matrix $\boldsymbol{Q}$, and

$$\begin{aligned}
\mu = {} & \mu_u + \mu_q + \mu_r + \alpha_2\delta_u p_{21}m_{11}^{-1}\left\|\boldsymbol{W}_u^*\right\|_F^2 \\
& + \alpha_2\delta_q p_{22}m_{55}^{-1}\left\|\boldsymbol{W}_q^*\right\|_F^2 \\
& + \alpha_2\delta_r p_{23}m_{66}^{-1}\left\|\boldsymbol{W}_r^*\right\|_F^2 + \alpha_2\kappa_u p_{21}m_{11}^{-1}\left|\eta_u^* - \eta_{u0}\right|^2 \\
& + \alpha_2\kappa_q p_{22}m_{55}^{-1}\left|\eta_q^* - \eta_{q0}\right|^2 + \alpha_2\kappa_r p_{23}m_{66}^{-1}\left|\eta_r^* - \eta_{r0}\right|^2
\end{aligned} \tag{45}$$

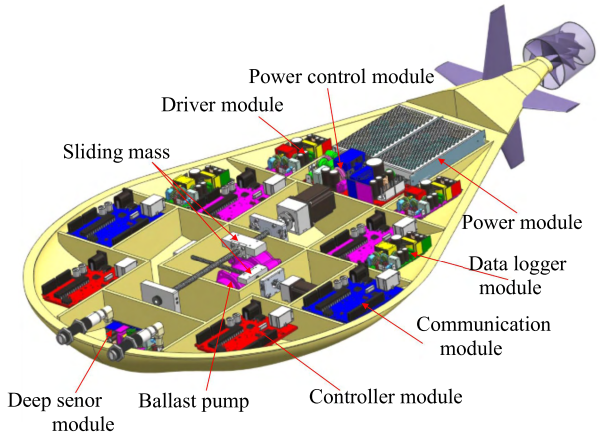

FIGURE 5. The configurations of flying-wing underactuated AUV.

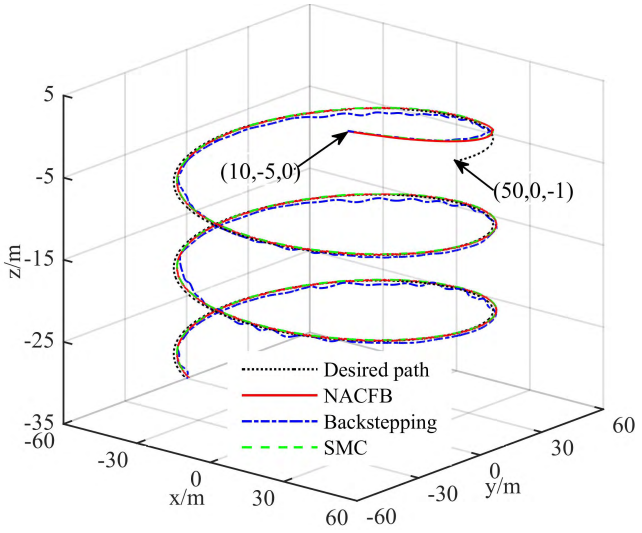

FIGURE 6. 3D path following of the flying-wing underactuated AUV.

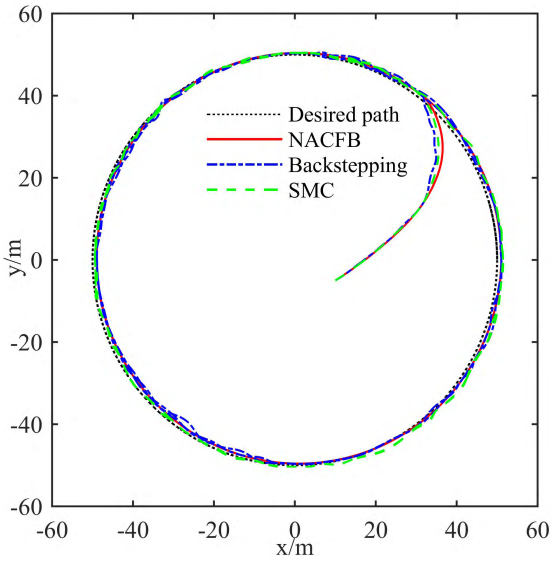

FIGURE 7. X-Y plane projection for the 3D path following of AUV.

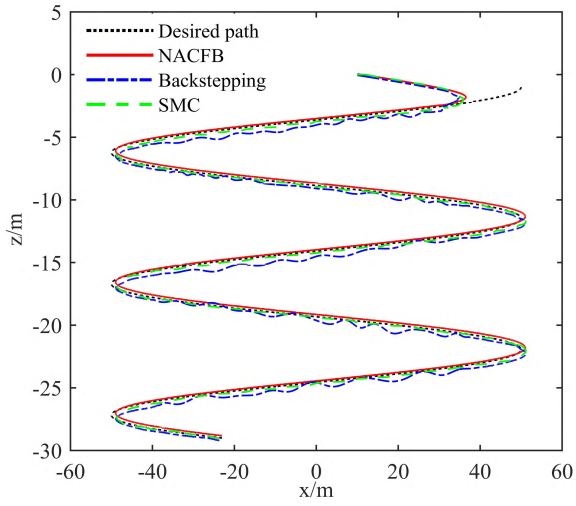

FIGURE 8. X-Z plane projection for the 3D path following of AUV.

This result implies that all the signals in the closed-loop control system are uniformly ultimately bounded, and the path following errors converge to a small neighborhood of the origin. This completes the proof.

V. SIMULATION EXAMPLES

In this section, numerical simulations are performed in MATLAB software environment to verify path following performance of the proposed control scheme. We conduct simulations on a new class of flying-wing underactuated AUV (Figure 5) designed by Harbin Institute of Technology in China, which has more excellent hydrodynamic properties compared with traditional AUVs. The model parameters are given in [37].

Initially, the three-dimensional desired spiral path is defined as:

$$\begin{cases} x_d(s) = 50\cos(0.6s) \\ y_d(s) = 50\sin(0.6s) \\ z_d(s) = -s - 1 \end{cases} \tag{46}$$

The initial position and attitude angle of a real AUV are given by $x(0) = 10m, y(0) = -5m, z(0) = 0m, \theta(0) = 0°$ and $\psi(0) = 45°$, and initial velocity matrix is $[u, v, w]^{\mathrm{T}} = 0m/s$. To verify robustness of the proposed controller, we assume that AUV is affected by the following environmental disturbances:

$$\boldsymbol{d}(t) + \boldsymbol{T}\dot{d}(t) = \boldsymbol{K}\omega \tag{47}$$

where $\boldsymbol{d}(t) = [d_u(t), d_v(t), d_w(t), d_q(t), d_r(t)]^{\mathrm{T}}$, ω is the white noise disturbance,and $\boldsymbol{K} = diag\{5, 4, 4, 5, 5\}$, $\boldsymbol{T} = diag\{5, 5, 5, 5, 5\}$

Meanwhile, AUV parameters are assumed to be unknown completely, and the unknown dynamics of the AUV is presented as follows:

$$f_k(k) = \delta_1 k + \delta_2 |k| k + \delta_3 k^3 \tag{48}$$

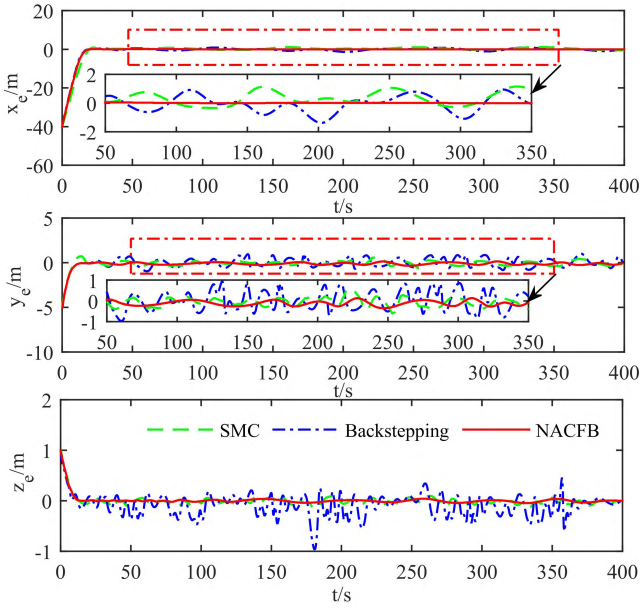

FIGURE 9. Three-dimensional path following errors of AUV.

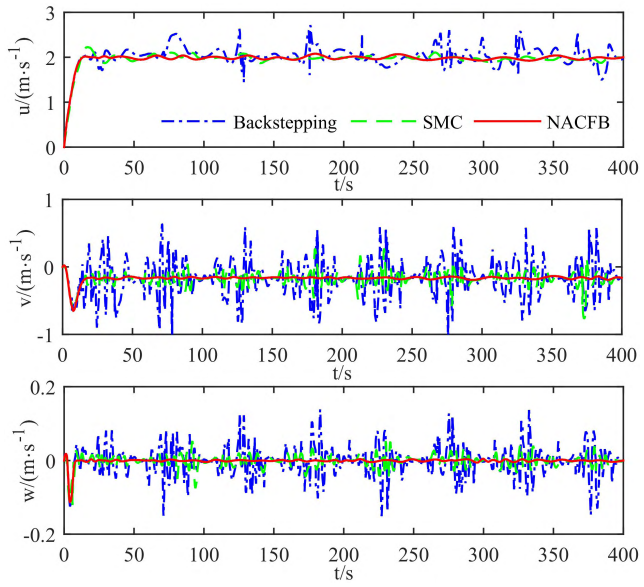

FIGURE 10. Velocity response curves of AUV.

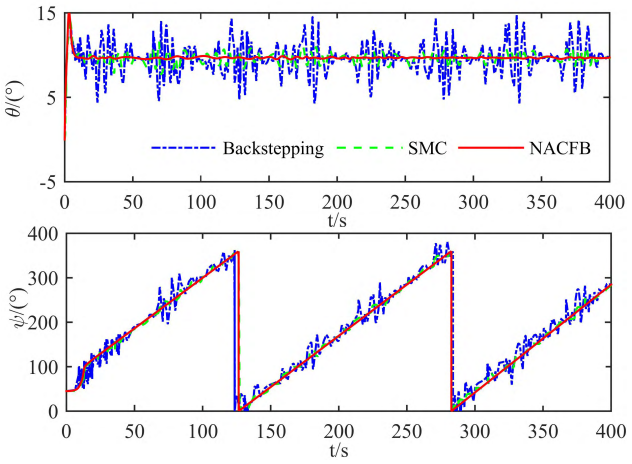

FIGURE 11. Angle response curves of AUV.

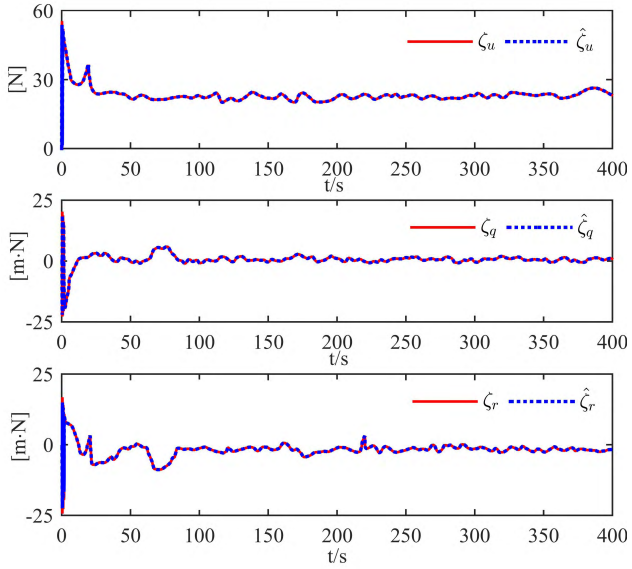

FIGURE 12. Estimated total uncertainties with RBF neural networks.

where $k = u, v, w, q, r$, and $\delta_1 = 0.6, \delta_2 = 0.3$, $\delta_1 = 0.2$.

The controller parameters are given by $\chi_s = 12$, $\chi_e = 6$, $\chi_h = 4$, $\chi_\psi = \chi_\theta = 6$, $\chi_u = 16$, $\chi_q = \chi_r = 8$, $\chi_{iu} = 5$, $\chi_{iq} = 3$, $\chi_{ir} = 3$, $p_{21} = 12, p_{22} = p_{23} = 6$.

Furthermore, the RBF neural networks with ten hidden nodes are used to approximate the uncertain dynamics of the AUV. The center vector and the standard deviation are chosen as $\boldsymbol{\mu}_n = [-10, -8, -6, -4, -2, 2, 4, 6, 8, 10]^T$ and $\lambda_n = 15$ based on the K clustering method [38], and the parameters of the RBF neural networks are $\lambda_{wu} = 12$, $\lambda_{wq} = 12$, $\lambda_{wr} = 12$, $\delta_u = 0.1$, $\delta_q = 0.1$, $\delta_r = 0.1$, $\lambda_{\eta u} = 8$, $\lambda_{\eta q} = 6$, $\lambda_{\eta r} = 6$, $\kappa_u = 1$,

$\kappa_q = 0.5$, $\kappa_r = 0.5$. Moreover, in order to filter out the high frequency measurement noise in the system, the shear frequency of the filter is given by $\varpi_n = 2\pi f = 20 rad/s$, where f is the actual operation frequency of AUV, which is usually $3 \sim 4$ Hz. The damping ratio is set to $\zeta = 0.95$ to guarantee that the system is overdamped.

Simulation results by using neuro-adaptive command filtered backstepping (NACFB) control, the sliding mode control (SMC) [39] and the traditional backstepping control are shown in Figures 6, 7, 8, 9, 10, 11, 12 and 13.

As can be seen from Figures 6, 7 and 8, compared with the traditional backstepping controller and the sliding mode controller, the proposed controller in this paper can more accurately complete the AUV three-dimensional path following in the presence of model perturbations and external

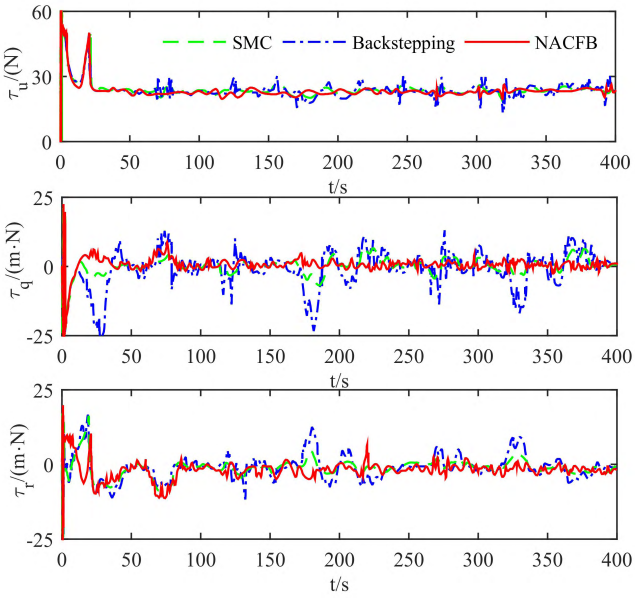

FIGURE 13. Control force and moments of AUV.

disturbances. And as shown in Figures 9, 10 and 11, the path following errors eventually converge to a small neighborhood of the zero under the NACFB controller, and the NACFB controller is not sensitive to the external disturbances, which indicates the proposed controller is of good robustness.

VI. CONCLUSIONS AND FUTUREWORK

In this paper, a neuro-adaptive command filtered back- stepping controller is presented for the three-dimensional path following problem of an underactuated AUV. A second-order filter is developed to obtain the derivative of virtual control, which greatly reduces the computational complexities of the traditional backstepping method, and filters out high frequency measurement noise in the system. Then, a filtered error compensation loop is designed to guarantee the approximation precision between the virtual control signals and the filtered signals. Moreover, all of vehicle uncertainties are compensated by the RBF neural networks and adaptive control techniques. And the stability of path following control system is proved based on the Lyapunov stability theory. Finally, simulations and comparative analysis were conducted to verify that the proposed controller is high accuracy of path following and good robustness.

For the futurework, path following of AUVs in the presence of constraints should be developed [40], and it is of interest to extend these results to the distributed path following of AUVs by using the distributed coordination method [41]–[42].

REFERENCES

[1] Y.-Y. Xu, Y.-J. Pang, Y. Gan, and Y.-Y. Sun, "AUV—State-of-the-art and prospect," *CAAI Trans. Intell. Syst.*, vol. 1, no. 1, pp. 9–16, 2006.
[2] Y. Xu and K. Xiao, "Technology development of autonomous ocean vehicle," *Acta Automat. Sinica*, vol. 33, no. 5, pp. 518–521, May 2007.
[3] C. Monique, "Autonomous underwater vehicles," *Ocean Eng.*, vol. 36, no. 1, pp. 1–2, 2009.
[4] R. B. Wynn *et al.*, "Autonomous underwater vehicles (AUVs): Their past, present and future contributions to the advancement of marine geoscience," *Mar. Geol.*, vol. 352, pp. 451–468, Jun. 2014.
[5] S. A. Villar, G. G. Acosta, A. L. Sousa, and A. Rozenfel, "Evaluation of an efficient approach for target tracking from acoustic imagery for the perception system of an autonomous underwater vehicle," *Int. J. Adv. Robot. Syst.*, vol. 11, no. 2, pp. 1–13, Feb. 2014.
[6] J. K. Pothal and D. R. Parhi, "Navigation of multiple mobile robots in a highly clutter terrains using adaptive neuro-fuzzy inference system," *Robot. Auton. Syst.*, vol. 72, pp. 48–58, Oct. 2015.
[7] T. B. Curtin, D. M. Crimmins, J. Curcio, M. Benjamin, and C. Roper, "Autonomous underwater vehicles: Trends and transformations," *Mar. Technol. Soc. J.*, vol. 39, no. 3, pp. 65–75, Sep. 2005.
[8] F. Wang, L. Wan, Y. Li, Y. M. Su, and Y. R. Xu, "A survey on development of motion control for underactuated AUV," *Shipbuild China*, vol. 51, no. 2, pp. 227–241, Feb. 2010.
[9] F. Zhang, G. Marani, R. N. Smith, and H. T. Choi, "Future trends in marine robotics," *IEEE Robot. Autom. Mag.*, vol. 22, no. 1, pp. 14–122, Mar. 2015.
[10] A. M. Lekkas and T. I. Fossen, "Integral LOS path following for curved paths based on a monotone cubic Hermite spline parametrization," *IEEE Trans. Control Syst. Technol.*, vol. 22, no. 6, pp. 2287–2301, Nov. 2014.
[11] O. Calvo, A. Rozenfeld, A. Souza, F. Valenciaga, P. F. Puleston, and G. Acosta, "Experimental results on smooth path tracking with application to pipe surveying on inexpensive AUV," in *Proc. Int. Conf. Intell. Robots Syst.*, Nice, France, Sep. 2008, pp. 3647–3653.
[12] N. Wang, Z. Sun, J. Yin, and Z. Zheng, "Surge-varying LOS based path following control of underactuated marine vehicles with accurate disturbance observation," in *Proc. IEEE Int. Conf. Underwater Syst. Technol., Theory Appl.*, Dec. 2017, pp. 1–6.
[13] J. Garus and B. Zak, "Using of soft computing techniques to control of underwater robot," in *Proc. Int. Conf. Methods Models Autom. Robot.*, Miedzyzdroje, Poland, Aug. 2010, pp. 415–419.
[14] E. Borhaug, A. Pavlov, and K. Y. Pettersen, "Integral LOS control for path following of underactuated marine surface vessels in the presence of constant ocean currents," in *Proc. 47th IEEE Conf. Decis. Control*, Cancun, Mexico, Dec. 2008, pp. 4984–4991.
[15] X. Liang, Y. You, L. F. Su, W. Li, and J. Zhang, "Path following control for underactuated AUV based on feedback gain backstepping," *Tech. Gazette*, vol. 22, no. 4, pp. 829–835, Aug. 2015.
[16] Z. Dong, L. Wan, Y. Li, T. Liu, and G. Zhang, "Trajectory tracking control of underactuated USV based on modified backstepping approach," *Int. J. Nav. Archit. Ocean Eng.*, vol. 7, no. 5, pp. 817–832, Sep. 2015.
[17] L. Liu, D. Wang, and Z. Peng, "Path following of marine surface vehicles with dynamical uncertainty and time-varying ocean disturbances," *Neurocomputing*, vol. 173, pp. 799–808, Jan. 2016.
[18] F. Repoulias and E. Papadopoulos, "Planar trajectory planning and tracking control design for underactuated AUVs," *Ocean Eng.*, vol. 34, nos. 11–12, pp. 1650–1667, Aug. 2007.
[19] X. Qi, "Spatial target path following control based on Nussbaum gain method for underactuated underwater vehicle," *Ocean Eng.*, vol. 104, pp. 680–685, Aug. 2015.
[20] N. Wang and M. J. Er, "Direct adaptive fuzzy tracking control of marine vehicles with fully unknown parametric dynamics and uncertainties," *IEEE Trans. Control Syst. Technol.*, vol. 24, no. 5, pp. 1845–1852, Sep. 2016.
[21] X. Liang, X. Qu, L. Wan, and Q. Ma, "Three-dimensional path following of an underactuated AUV based on fuzzy back-stepping sliding mode control," *Int. J. Fuzzy Syst.*, vol. 20, no. 2, pp. 640–649, Sep. 2016.
[22] N. Wang, M. J. Er, J.-C. Sun, and Y.-C. Liu, "Adaptive robust online constructive fuzzy control of a complex surface vehicle system," *IEEE Trans. Cybern.*, vol. 46, no. 7, pp. 1511–1523, Jul. 2016.
[23] N. Wang, C. Qian, J.-C. Sun, and Y.-C. Liu, "Adaptive robust finite-time trajectory tracking control of fully actuated marine surface vehicles," *IEEE Trans. Control Syst. Technol.*, vol. 24, no. 4, pp. 1454–1462, Jul. 2016.
[24] Z. Zheng and L. Sun, "Path following control for marine surface vessel with uncertainties and input saturation," *Neurocomputing*, vol. 177, pp. 158–167, Sep. 2016.
[25] B. Xu, Z. Shi, C. Yang, and F. Sun, "Composite neural dynamic surface control of a class of uncertain nonlinear systems in strict-feedback form," *IEEE Trans. Cybern.*, vol. 44, no. 12, pp. 2626–2634, Dec. 2014.

[26] X. Xiang, C. Yu, and Q. Zhang, "On intelligent risk analysis and critical decision of underwater robotic vehicle," *Ocean Eng.*, vol. 140, pp. 453–465, Aug. 2017.
[27] W. Caharija, K. Y. Pettersen, J. T. Gravdahl, and E. Børhaug, "Path following of underactuated autonomous underwater vehicles in the presence of ocean currents," in *Proc. 51st IEEE Conf. Decis. Control*, Maui, HI, USA, Dec. 2012, pp. 528–535.
[28] T. I. Fossen, K. Y. Pettersen, and R. Galeazzi, "Line-of-sight path following for Dubins paths with adaptive sideslip compensation of drift forces," *IEEE Trans. Control Syst. Technol.*, vol. 23, no. 2, pp. 820–827, Mar. 2015.
[29] H.-J. Wang, Z.-Y. Chen, H.-M. Jia, and J. Li, "Three-dimensional path-following control of underactuated unmanned underwater vehicle using feedback gain backstepping," *Control Theory Appl.*, vol. 31, no. 1, pp. 66–77, Jan. 2014.
[30] H. J. Wang, Z. Y. Chen, H. M. Jia, and X. H. Chen, "Under actuated AUV 3D path tracking control based filter backstepping method," *Acta Automat. Sinica*, vol. 41, no. 3, pp. 631–645, 2015.
[31] Y. Wang, M. Zhang, P. A. Wilson, and X. Liu, "Adaptive neural network-based backstepping fault tolerant control for underwater vehicles with thruster fault," *Ocean Eng.*, vol. 110, pp. 15–24, Dec. 2015.
[32] K. Shojaei, "Observer-based neural adaptive formation control of autonomous surface vessels with limited torque," *Robot. Auton. Syst.*, vol. 78, pp. 83–96, Apr. 2016.
[33] K. D. Do, "Coordination control of underactuated ODINs in three-dimensional space," *Robot. Auton. Syst.*, vol. 61, no. 8, pp. 853–867, Aug. 2013.
[34] K. Y. Pettersen and O. Egeland, "Time-varying exponential stabilization of the position and attitude of an underactuated autonomous underwater vehicle," *IEEE Trans. Autom. Control*, vol. 44, no. 1, pp. 112–115, Jan. 1999.
[35] X. Xiang, C. Yu, and Q. Zhang, "Robust fuzzy 3D path following for autonomous underwater vehicle subject to uncertainties," *Comput. Oper. Res.*, vol. 84, pp. 165–177, Aug. 2017.
[36] J. A. Farrell, M. Polycarpou, M. Sharma, and W. Dong, "Command filtered backstepping," *IEEE Trans. Autom. Control*, vol. 54, no. 6, pp. 1391–1395, Jun. 2009.
[37] J. Q. Wang, C. Wang, Y. J. Wei, and C. J. Zhang, "Hydrodynamic characteristics and motion simulation of flying-wing dish-shaped autonomous underwater glider," *Harbin Inst. Technol.*, vol. 50, no. 4, pp. 131–137, Apr. 2018.
[38] M.-J. Zhang and Z.-Z. Chu, "Adaptive sliding mode control based on local recurrent neural networks for underwater robot," *Ocean Eng.*, vol. 45, no. 1, pp. 56–62, May 2012.
[39] H. M. Jia, L. J. Zhang, X. Q. Cheng, X. Q. Bian, Z. P. Yan, and J. J. Zhou, "Three-dimensional path following control for an underactuated UUV based on nonlinear iterative sliding mode," *Acta Automat. Sinica*, vol. 38, no. 2, pp. 308–314, Feb. 2012.
[40] Z. Peng, J. Wang, and J. Wang, "Constrained control of autonomous underwater vehicles based on command optimization and disturbance estimation," *IEEE Trans. Ind. Electron.*, vol. 64, no. 5, pp. 3831–3839, Jul. 2018.
[41] Z. Peng and J. Wang, "Output-feedback path-following control of autonomous underwater vehicles based on an extended state observer and projection neural networks," *IEEE Trans. Syst., Man, Cybern. Syst.*, vol. 48, no. 4, pp. 535–544, Apr. 2018.
[42] Z. Peng, J. Wang, and D. Wang, "Distributed maneuvering of autonomous surface vehicles based on neurodynamic optimization and fuzzy approximation," *IEEE Trans. Control Syst. Technol.*, vol. 26, no. 3, pp. 1083–1090, May 2018.

JINQIANG WANG was born in Harbin, China. He received the B.E. degree in naval architecture and ocean engineering from the School of Shipbuilding Engineering, Harbin Engineering University, Harbin, China, in 2016. He is currently pursuing the Ph.D. degree in astronautics with the Harbin Institute of Technology. His current research interests include guidance and the motion control of autonomous underwater vehicles.

CONG WANG received the bachelor's and master's degrees in mechanical and electrical engineering from Northeast Forestry University in 1989 and 1993, respectively, and the Ph.D. degree in mechanics from the Harbin Institute of Technology, Harbin, China, in 2001. He is currently a Professor with the School of Astronautics, Harbin Institute of Technology, China. His current research interests include fluid mechanics and the motion control of underwater vehicles.

YINGJIE WEI received the bachelor's and master's degrees in oil and gas field development from Northeast Petroleum University in 1996 and 2000, respectively, and the Ph.D. degree in mechanics from the Harbin Institute of Technology, Harbin, China, in 2003. He is currently a Professor with the School of Astronautics, Harbin Institute of Technology, China. His current research interests include multiphase fluid mechanics and hydrodynamics of the underwater vehicles.

CHENGJU ZHANG received the B.E. degree in naval architecture and ocean engineering from the School of Shipbuilding Engineering, Harbin Engineering University, Harbin, China, in 2017. He is currently pursuing the Ph.D. degree in astronautics with the Harbin Institute of Technology. His current research interests include the motion control of marine surface vehicles.